Free Radical Biology and Medicine 194 (2023) 42–51

Contents lists available at ScienceDirect

Free Radical Biology and Medicine

journal homepage: www.elsevier.com/locate/freeradbiomed

Singlet oxygen and radical-mediated mechanisms in the oxidative cellular damage photosensitized by the protease inhibitor simeprevir

Guillermo Garcia-Lainez [a,1], Meryem El Ouardi [b,c,1], Alejandro Moreno [a], Emilio Lence [d], Concepción González-Bello [d], Miguel A. Miranda [b,c,**], Inmaculada Andreu [b,c,*]

[a] Instituto de Investigación Sanitaria (IIS) La Fe, Hospital Universitari i Politècnic La Fe, Avenida de Fernando Abril Martorell 106, 46026, Valencia, Spain
[b] Departamento de Química-Instituto de Tecnología Química UPV-CSIC. Universitat Politècnica de València, Camino de Vera s/n, 46022, Valencia, Spain
[c] Unidad Mixta de Investigación UPV- IIS La Fe, Hospital Universitari i Politècnic La Fe, Avenida de Fernando Abril Martorell 106, 46026, Valencia, Spain
[d] Centro Singular de Investigación en Química Biolóxica e Materiais Moleculares (CiQUS), Departamento de Química Orgánica, Universidade de Santiago de Compostela, Jenaro de la Fuente s/n, 15782, Santiago de Compostela, Spain

ARTICLE INFO

Keywords:
Antiviral agent
Binding to proteins
Cellular photo(geno)toxicity
Photodamage to biomolecules
Triplet excited state

ABSTRACT

Hepatitis C, a liver inflammation caused by the hepatitis C virus (HCV), is treated with antiviral drugs. In this context, simeprevir (SIM) is an NS3/4A protease inhibitor used in HCV genotypes 1 and 4. It is orally administered and achieves high virological cure rates. Among adverse reactions associated with SIM treatment, photosensitivity reactions have been reported. In the present work, it is clearly shown that SIM is markedly phototoxic, according to the *in vitro* NRU assay using BALB/c 3T3 mouse fibroblast. This result sheds light on the nature of the photosensitivity reactions induced by SIM in HCV patients, suggesting that porphyrin elevation in patients treated with SIM may not be the only mechanism responsible for SIM-associated photosensitivity. Moreover, lipid photoperoxidation and protein photooxidation assays, using human skin fibroblasts (FSK) and human serum albumin (HSA), respectively, reveal the capability of this drug to promote photodamage to cellular membranes. Also, DNA photo lesions induced by SIM are noticed through comet assay in FSK cells. Photochemical and photobiological studies on the mechanism of SIM-mediated photodamage to biomolecules indicate that the key transient species generated upon SIM irradiation is the triplet excited state. This species is efficiently quenched by oxygen giving rise to singlet oxygen, which is responsible for the oxidation of lipids and DNA (Type II mechanism). In the presence of HSA, the photobehavior is dominated by binding to site 3 of the protein, to give a stable SIM@HSA complex. Inside the complex, quenching of the triplet excited state is less efficient, which results in a longer triplet lifetime and in a decreased singlet oxygen formation. Hence, SIM-mediated photooxidation of the protein is better explained through a radical (Type I) mechanism.

1. Introduction

Hepatitis C virus (HCV) infection is a health service problem of the first magnitude in Europe and especially in the Mediterranean countries, where prevalence rates are in the range 1–3% [1–3]. Moreover, hepatitis C can lead to liver cirrhosis and liver cancer, being a leading cause of liver transplantation [4].

Simeprevir (SIM) is an NS3/4A protease inhibitor for use in HCV genotypes 1 and 4. It is orally administered and achieves high virological cure rates. Moreover, it has a favorable tolerability profile when used in combination with peginterferon-alfa plus ribavirin or with sofosbuvir [5–8].

Recently, it has been reported that SIM is an especially promising drug for treating COVID-19 because it potently reduces SARS-CoV-2 viral load by multiple orders of magnitude [9,10]. In this context, the viral protease inhibitors nelfinavir and simeprevir revealed good plasma exposures and based on their described mode of action, they may inhibit SARS-CoV-2 directly [11]. Therefore, SIM could prevent coronavirus

* Corresponding author. Departamento de Química-Instituto de Tecnología Química UPV-CSIC. Universitat Politècnica de València, Camino de Vera s/n, 46022, Valencia, Spain.
** Corresponding author. Departamento de Química-Instituto de Tecnología Química UPV-CSIC. Universitat Politècnica de València, Camino de Vera s/n, 46022, Valencia, Spain.
E-mail addresses: mmiranda@qim.upv.es (M.A. Miranda), iandreur@qim.upv.es (I. Andreu).
[1] These authors equally contributed to the work.

https://doi.org/10.1016/j.freeradbiomed.2022.11.006
Received 29 July 2022; Received in revised form 4 October 2022; Accepted 6 November 2022
Available online 12 November 2022

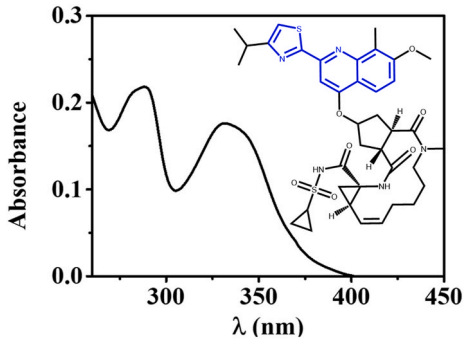

Fig. 1. Absorption spectrum of SIM in PBS. Inset: Chemical structure of SIM.

from replicating and might help in Covid-19 treatment.

The most commonly occurring adverse events associated with SIM treatment are rash, itching, sun sensitivity, muscle pain, shortness of breath, and nausea [5,12–14]. In particular, photosensitivity reactions have been reported in phase III studies [15]. Moreover, dermatological side-effects could be a problem in the management of SIM administration, and pharmacokinetic analysis is a valuable tool in a "real-life" clinical setting. In a previous study, it has been evaluated a possible relationship between plasma levels and the onset of skin complaints. With regard to this, SIM plasma concentrations were significantly related to dermatological side effects at early time points and the best predictive factor for skin symptoms was simeprevir concentrations at one week. Photosensitive condition (grade-1 sunburn) was found after the first month [16].

In this context, SIM is associated with phototoxicity, but there is no clear evidence for an increased risk of keratinocyte carcinoma [17]. Thus, SIM would act as a light-activated photosensitizer triggering a cascade of chemical events that may finally result in important biological disorders. This damage would occur by direct modification of biomolecules (isomerization, bond breaking, oxidation, etc.) or through the involvement of free radical intermediates, including singlet oxygen. As a result, cell constituents such as unsaturated lipids, proteins, or bases of nucleic acids can be altered. In this situation, if the repair mechanisms are not efficient, there can be irreversible lesions.

Given the above, a better understanding of the photodermatologic adverse reactions of SIM, based on a thorough photochemical and photobiological mechanistic study is necessary.

With this background, the aim of the present work is to investigate the direct photodamage to cells induced by SIM itself, using a methodology previously set up in our group to study photosensitivity reactions [18–21]. This makes sense since SIM displays a significant absorption band in the UVA region, which is an active fraction of solar light able to produce photosensitivity disorders. As shown in Fig. 1, the spectrum has two maxima centered at 288 nm and 332 nm that correspond to the thiazole-quinoline chromophore (Fig. 1). After light absorption by SIM, highly reactive intermediates could be formed including organic radicals and reactive oxygen species (ROS). Short-lived transients of these types could be in the origin of the clinically observed photosensitivity reactions.

2. Material and methods

2.1. General

Experimental descriptions such as chemicals and reagents, irradiation equipment, spectroscopic measurements, cell culture conditions, data analysis and statistics are provided in the supplementary material.

2.2. Laser flash photolysis

Laser flash photolysis (LFP) measurements were performed using a pulsed Nd:YAG L52137 V LOTIS TII laser at 355 nm as the excitation wavelength (Sp Lotis Tii, Minsk, Belarus). The LFP equipment consisted of a pulsed laser, a 77 250 Oriel monochromator, and an oscilloscope DP04054 Tektronix. The single pulses were ~10 ns of duration, and the energy was ~12 mJ/pulse. For processing, the output signal from the oscilloscope was transferred to a personal computer. The measurements were recorded under aerated atmosphere, or in the case of triplet excited state decays, the solutions were deaerated by bubbling nitrogen (15 min). The absorbance of the samples was adjusted at ~0.30 at 355 nm and the rate constant of triplet excited state quenching by oxygen (k_q) was determined using the Stern–Volmer equation (eq. (1)).

$$\frac{1}{\tau} = \frac{1}{\tau_0} + k_q\,[O_2] \qquad \text{eq.1}$$

Where τ and τ_0 are the lifetime of transient species with and without quencher (O_2), respectively.

For the rate constant of triplet excited state quenching by 2-methyl-cyclohexa-2,5-dienecarboxyl acid (MBA), the following Stern–Volmer equation (eq. (2)) was used:

$$\frac{1}{\tau} = \frac{1}{\tau_q} + k_q\,[MBA] \qquad \text{eq.2}$$

Where τ and τ_q are the lifetime of transient species in the presence and absence of MBA, respectively. Concentrations between 0.1 and 3 mM were used for MBA.

The rate constant of triplet excited state quenching by lapatinib (LAP) was calculated using the next Stern–Volmer equation (eq. (3)):

$$\frac{1}{\tau} = \frac{1}{\tau_q} + k_q\,[LAP] \qquad \text{eq.3}$$

Where τ and τ_q are the lifetime of transient species in the presence and absence of LAP, respectively. Concentrations up to 3 mM were used for the quencher.

Singlet oxygen ($^1O_2$, $^1\Delta g$) species was detected by NIR emission upon excitation with the Nd:YAG L52137 V LOTIS TII laser at 355 nm in aerated atmosphere. The absorbance of samples was adjusted at ~0.55 at 355 nm and decay traces were recorded at 1274 nm. Tetramethyl-*p*-benzoquinone (DQ) was used as a standard with a $^1O_2$ quantum yield (Φ_Δ) in MeCN, *ca.* 0.89 [22]. The Φ_Δ of SIM was calculated following equation (4).

$$\Phi_\Delta^{SIM} = \Phi_\Delta^{DQ} \times \frac{A_{SIM}}{A_{DQ}} \times \frac{I_{MeCN}}{I_i} \qquad \text{eq.4}$$

Where Φ_Δ^{DQ} is the quantum yield of the standard (DQ), A_{SIM} and A_{DQ} are the absorbances of SIM and DQ, I_{MeCN} and I_i the refractive index of acetonitrile and the sample solvent, respectively.

All transient absorption experiments were performed in PBS, MeOH or MeCN at room temperature.

2.3. In vitro 3T3 neutral red uptake (NRU) phototoxicity test

The *in vitro* 3T3 NRU phototoxicity assay was basically performed according to the OECD Guideline 432 [23] as described in Garcia-Lainez et al. [19]. As positive and negative control were selected chlorpromazine (CPZ) and sodium dodecyl sulphate (SDS), respectively. In brief, two 96-well plates were seeded at a density of 2.5×10^4 cells/well. Then, serial dilutions of the drug ranging from 100 μM to 0.25 μM were added to each plate. After 1 h incubation at 37 °C in dark conditions, one plate was irradiated with a non-cytotoxic UVA light dose of 5 J/cm^2 whereas the other one was kept in the dark. Once UVA irradiation finished, culture medium was replaced, and plates were incubated overnight. Next day, 50 μg/mL neutral red solution was added into each well and incubated for 2 h at 37 °C. Cells were then washed once with PBS. In order to extract neutral red from lysosomes, 100 μL of desorption

solution (50% distilled water, 49.5% absolute ethanol and 0.5% acetic acid) was added per well. Absorbance was measured at 550 nm on a Synergy H1 microplate reader. Dose-response curves were established for each compound to determine the concentration producing a 50% decrease in the neutral red uptake (IC50) in dark and UVA light conditions by non-lineal regression methods using the Graph Pad 5.0 software. Finally, photoirritant factor (PIF) values were calculated according to equation (5).

$$PIF = \frac{IC50\ DARK}{IC50\ UVA\ LIGHT} \quad \text{eq.5}$$

As stated in the OECD Guideline 432, a compound is labeled as "non-phototoxic" when PIF is < 2, "probably phototoxic" if PIF is between 2 and 5 and "phototoxic" if PIF is > 5.

2.4. Photoinduced lipid peroxidation assay

The compound 4,4-difluoro-5-(4-phenyl-1,3-butadienyl)-4-bora-3a,4a-diaza-*s*-indacene-3-undecanoic acid, also known as C11-Bodipy 581/591 is a molecular probe to assess lipid peroxidation in living cells that shifts its fluorescence from red to green when the molecule is oxidized [24,25]. To this end, human skin fibroblast cells (FSK) were seeded in two 12-well-plates at a density of 6.0×10^4 cells/well. Next day, the cells were treated with 5 μM of SIM solutions and incubated for 30 min in dark conditions. After incubation, one plate was irradiated (2.5 J/cm^2) and the other one was kept in dark conditions as negative control. Cells were labeled with the lipid peroxidation sensor C11 Bodipy 581/591 (10 μM) for 30 min at 37 °C. Finally, the cultures were visualized using a Leica DMI 4000B fluorescence microscope in sequential mode to detect both the non-oxidized (red fluorescence, λ_{exc} 535 nm) and the oxidized (green fluorescence, λ_{exc} 490 nm) forms of the probe. To determine the extent of lipid peroxidation in each condition, the fluorescence intensity ratio (FIR) was calculated following equation (6) using the Image-J software image analyzer (NIH).

$$FIR = \frac{I\ red\ fluorescence}{I\ green\ fluorescence} \quad \text{eq.6}$$

2.5. Protein photooxidation assay

Protein oxidation photoinduced by SIM, using human serum albumin (HSA) as model, was evaluated as previously described [26] with minor modifications. In brief, HSA solutions in PBS were prepared (5 mg/mL, 1 mg/sample) and incubated with increasing concentrations of SIM (1 μM, 2.5 μM and 5 μM) at room temperature for 1 h. Then, mixtures were irradiated with a UVA dose of 10 J/cm^2 or maintained in dark conditions as control of the assay. Immediately after irradiation, the extent of HSA oxidation was measured in all experimental conditions spectrophotometrically by derivatization with 2,4-dinitrophenylhydrazine (DNPH). Thus, 200 μL of DNPH (10 mM) was added and incubated at room temperature for 1 h to form stable dinitrophenyl hydrazone adducts. Proteins were then precipitated with a 20% (v/v) trichloroacetic (TCA) solution and incubated on ice for 15 min. Afterwards, pellets were washed twice with ethanol/ethyl acetate 1:1 (v/v) containing 20% TCA to remove the unbound DNPH and dried at 60 °C. The adducts were resolubilized in 100 μL of 6 M guanidine-hydrochloride at 4 °C by overnight incubation. Finally, absorbance at 375 nm was recorded using the Synergy H1 microplate reader and the HSA oxidation degree was expressed as nmol of carbonyl moiety per mg protein.

2.6. Assessment of DNA photodamage

2.6.1. Plasmid DNA photosensitized damage

Samples containing 250 ng of supercoiled circular DNA (pBR322, 4361 base pairs) in the presence or absence of SIM (100 μM) in PBS supplemented with 1 mg/mL HSA were prepared. Mixtures were irradiated as described above using a UVA light dose of 15 J/cm^2 (30 min). Immediately, loading buffer (0.25% bromophenol blue and 30% glycerol, in water) was added to each sample. Moreover, to characterize chemical modifications towards DNA bases promoted by the drug, samples were digested after irradiation with an excess of Endo V, Endo III or FPG (0.5 U) at 37 °C for 1 h and then, loading buffer was added as detailed above. Afterwards, all samples were loaded on a 0.8% agarose gel containing SYBR® Safe as nucleic acid stain. Electrophoresis run was carried out in TAE Buffer (0.04 M Tris-acetate, 1 mM EDTA) at 100 V for 2 h. DNA bands were visualized with the Gel Logic 200 Imaging System (Kodak) and densitometry was quantified with the Image-J software. Thus, the relative percentage of the nicked relaxed form (Form II) of the pBR322 plasmid was calculated for each condition.

2.6.2. 8-Oxo-dG quantitation assay as a biomarker of oxidative DNA damage

FSK cells were seeded in two 24-well plates at a density of 7.5×10^5 cells/well. Next day, they were treated with 2.5 μM SIM solutions for 30 min at 4 °C in dark conditions. After incubation, one plate was irradiated (2.5 J/cm^2) and the other one was kept in darkness. Afterwards, cells were harvested from the plates and then genomic DNA extraction was performed in all samples according to the manufacturer's protocol. DNA samples were quantified using a Nanodrop 2000c (Thermo Scientific). Later, samples containing 2 μg DNA (100 ng/mL) were digested with DNase I (1 U) at 37 °C for 1 h, followed by alkaline phosphatase incubation (1 U) at 37 °C for 1 h. Lastly, 8-oxo-dG concentration was determined in all samples by a competitive Elisa assay following the manufacturer's instructions. Data were expressed in nanomoles of 8-oxo-dG formed by interpolating the sample concentrations from the standard curve.

2.6.3. Nuclear DNA photodamage by comet assay

Single cell gel electrophoresis assay (comet assay) was carried out as previously described [20] in order to detect strand breaks and alkaline labile sites on nuclear DNA. Briefly, FSK cells were trypsinized, resuspended in cold PBS and allowed to stand for 2 h at 4 °C for repairing the damage generated after detachment with trypsin. Then, two 24-well plates were seeded at a density of 1.0×10^5 cells/well and treated with 2.5 μM SIM solution for 30 min at 4 °C in dark conditions. In this assay, CPZ (10 μM) was selected as the photogenotoxic reference compound. After incubation, one plate was placed in the photoreactor to irradiate the cells (2.5 J/cm^2) and the other one was kept in dark conditions as negative control. Immediately, irradiated and non-irradiated cells were harvested from the plates. Then, 100 μL of each sample was homogenized with 100 μL of 1% low melting point agarose solution and mixtures were placed forming drops (2.0×10^4 cell/gel) onto Trevigen® treated slides, allowing their jellification. Next, slides were immediately immersed in a container filled with lysis buffer (2.5 M NaCl, 0.1 M Na_2EDTA, 0.01 M Tris, 1% Triton X-100) and incubated overnight at 4 °C. In DNA recovery experiments to promote intrinsic cellular DNA-repair mechanisms, slides were maintained in DMEM medium at 37 °C for 20 h, and then lysed as stated above. Next day, all slides were transferred to a Trevigen® comet assay electrophoresis tank and covered with cold alkaline buffer (0.2 M NaOH, 1 mM EDTA, pH $\geq$ 13) and let during 40 min for DNA unwinding at 4 °C. Afterwards, the electrophoresis was carried out at 21 V (1 V/cm) for 30 min at 4 °C. Once the electrophoresis finished, the slides were washed twice in PBS for 5 min. DNA was fixed by two subsequent incubations with 70% and 100% ethanol solutions. Then, DNA was stained with SYBR Gold® (1:10.000 dilution in TE buffer – Tris-HCl 10 mM pH 7.5, EDTA 1 mM) for 30 min at 4 °C in darkness. Finally, the slides were air-dried and kept in dark conditions. Comet nucleoids and tails were visualized using a Leica DMI 4000B fluorescence microscope (λ_{exc} 490 nm). At least 100 cells/sample were analyzed to determine DNA damage. The percentage of DNA damage of each sample was calculated with the visual scoring of at least 100 DNA comets using the subsequent formula [27]: [(Nclass 0 comets

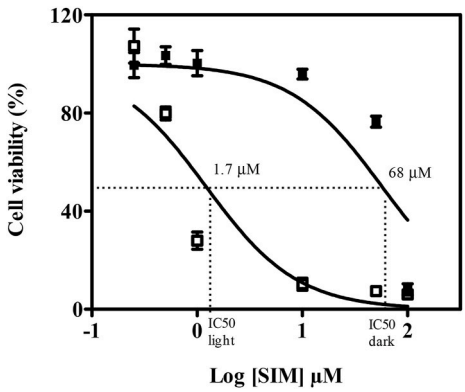

Fig. 2. 3T3 NRU phototoxicity assay. Dose-response curves for cell viability of BALB/c 3T3 mouse fibroblast cells treated with SIM in Dark (■) and UVA light conditions (5 J/cm^2, □). Data are the mean ± SD from four independent experiments.

× 0) + (Nclass 1 comets × 1) + (Nclass 2 comets × 2) + (Nclass 3 comets × 3) + [(Nclass 4 comets × 4) + (Nclass 5 comets × 5) + (Nclass 6 comets × 6)]/6, where class 0 comets indicate comets with no DNA damage and class 6 comets indicate comets with maximum DNA damage.

2.7. Molecular docking

These studies were carried out using our previously reported protocol for lapatinib against HSA [28,29]. The protein coordinates obtained in the crystal structure of HSA in complex with hemin and myristic acid (PDB entry 1O9X) [30] and the docking program GOLD version 2020.2.0 [31] were used.

2.8. Molecular dynamics simulation studies

The highest score solution obtained by docking was subjected to 100 ns of dynamic simulation, which was performed as previously described by us for trifusal [32]. The cpptraj module in AMBER 17 was used to analyze the trajectories and to calculate the rmsd of the protein and the ligand during the simulation [33]. The molecular graphics program PyMOL (DeLano) was employed for visualization and depicting enzyme structures.

3. Results and discussion

3.1. Phototoxicity of simeprevir

Sunlight activated drug can trigger a cascade of chemical events that finally result in important biological disorders including phototoxicity. This process can be evaluated through *in vitro* 3T3 NRU phototoxicity test following the OECD Guideline 432 [23].

3.1.1. In vitro 3T3 neutral red uptake (NRU) phototoxicity assay

Assessment of the phototoxicity of simeprevir (SIM) was performed according to the *in vitro* 3T3 NRU phototoxicity test [23]. To achieve this goal, BALB/c 3T3 mouse fibroblast cells were treated with increasing concentrations of SIM and cell viability was analyzed by neutral red as vital stain. From dose-response curves, half maximal inhibitory concentrations (IC50) under dark or UVA light conditions were estimated. As shown in Fig. 2, SIM displayed a cytotoxic profile in dark conditions with an IC50 in the micromolar range (68 µM). It is noteworthy that its toxicity was enhanced in combination with UVA light (IC50 = 1.7 µM). Consequently, phototoxicity was determined by the calculation of the photoirritant factor value (PIF), defined as the ratio between the IC50 under dark and light conditions. The PIF obtained was around 40, which is 8-fold higher than the cut-off value for a phototoxic compound as stated by the OECD guide [23]. Remarkably, this result sheds light on the nature of the photosensitivity reactions induced by SIM in HCV patients. So, it confirms that porphyrin elevation in patients treated with SIM may not be the only mechanism responsible for SIM-associated photosensitivity. Thus, phototoxic mechanisms usually comprise the generation of cellular oxidative stress that promotes damage to biomolecules such as lipids, proteins and DNA, leading ultimately to cell

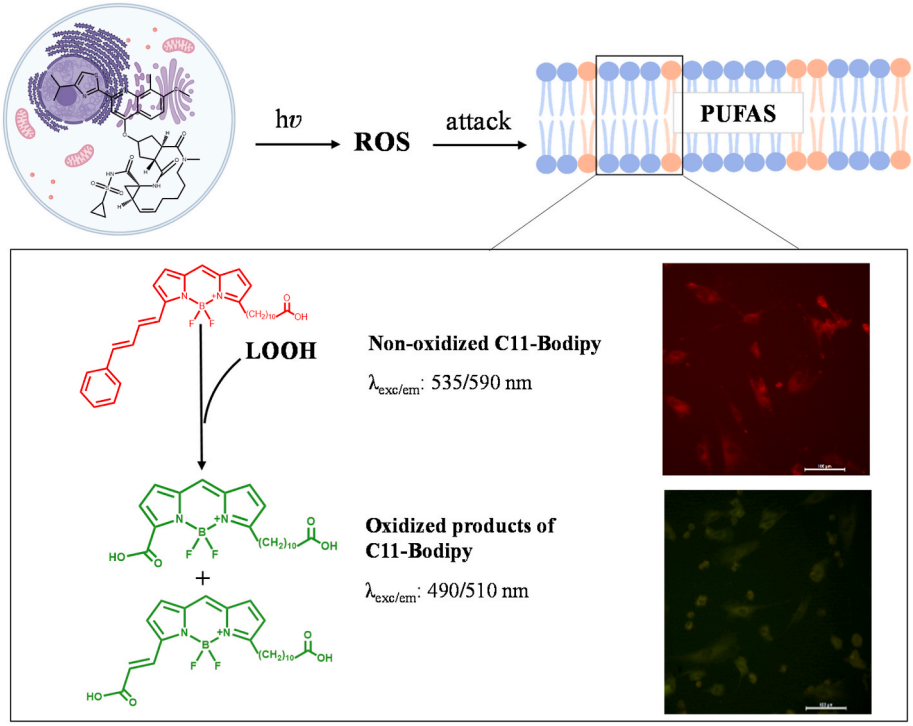

Scheme 1. Lipid photoperoxidation detection in human skin fibroblast cells (FSK) by C11-BODIPY (581/591) probe.

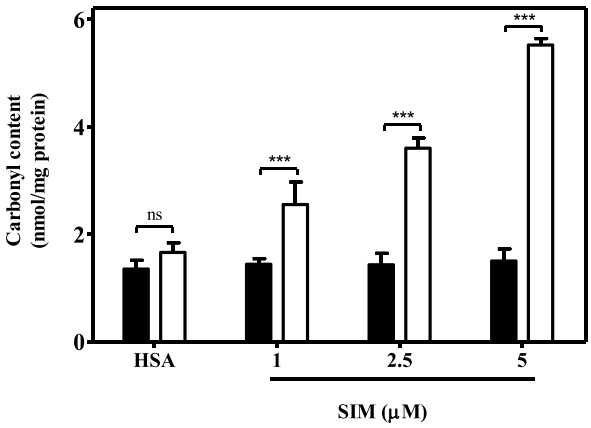

Fig. 3. Protein photooxidation promoted by SIM in human serum albumin (HSA) model. HSA was irradiated (10 J/cm^2) in the presence of SIM and the carbonyl content was evaluated spectrophotometrically by monitoring its carbonyl moiety after derivatization with 2,4-dinitrophenylhydrazine ($\lambda = 375$ nm). Non-irradiated solutions were analyzed as control (■). Data are the mean ± SD of three independent experiments. Asterisks show significant differences by the Student's t-test compared to dark conditions (***$p < 0.001$, ns: non-significant).

death [34].

3.1.2. Lipid and protein photooxidation

As SIM displays highly lipophilic properties, membrane components (lipids and proteins) could be the targets for its phototoxicity. To confirm this hypothesis, first, lipid photoperoxidation was investigated using the fluorescent reporter C11-Bodipy 581/591, which consists of a boron dipyrromethene difluoride core attached to a fatty acid tail and a phenyl moiety connected by a diene bond (Scheme 1). This assay is based on the capability of this molecular probe to penetrate the plasmatic membrane and to shift the fluorescence emission upon its oxidation from red (λ_{exc} 535 nm), which corresponds to the native structure of the probe, to green (λ_{exc} 490 nm), attributed to its oxidation products. As it is described in the literature, the Bodipy is exclusively sensitive to free radical species generated from hydroperoxides, but not to hydroperoxides *per se* [35,36]. With this aim, FSK cells were treated with SIM (5 μM) and subsequently irradiated (2.5 J/cm^2) or maintained in darkness as control. Then, cells were stained with the C11-Bodipy 581/591 after irradiation to rule out direct photochemical reactions between the drug and the probe, and finally, they were visualized under the fluorescent microscope. The images shown in Scheme 1 and Fig. S1 revealed an increase in the green fluorescence intensity (oxidized product) in UVA light conditions in comparison with non-irradiated treated cells, indicating a high degree of lipid peroxidation. By contrast, lipid peroxidation in non-treated cells was negligible. Accordingly, the quantitative analysis showed a significant reduction of the red to green fluorescence intensity ratio (Fig. S1). These results support that lipid membrane is indeed a potential target for SIM phototoxicity.

Moreover, protein photooxidation was investigated using the human serum albumin (HSA) as protein model. Thus, solutions of HSA containing SIM were UVA irradiated with a dose of 10 J/cm^2 and afterwards, the carbonyl moiety, as a biomarker of protein oxidation, was quantified by the derivatization method using 2,4-dinitropheynlhydrazine (DNPH). According to Fig. 3, irradiated HSA without treatment showed similar concentration of carbonyl moiety as non-irradiated HSA, indicating the suitability of the dose selected. Interestingly, for SIM, a dose-dependent enhancement of the carbonyl content of HSA was observed after irradiation in comparison with non-irradiated mixtures, reaching *ca.* 3-fold increase at 5 μM. This assay confirmed the capability

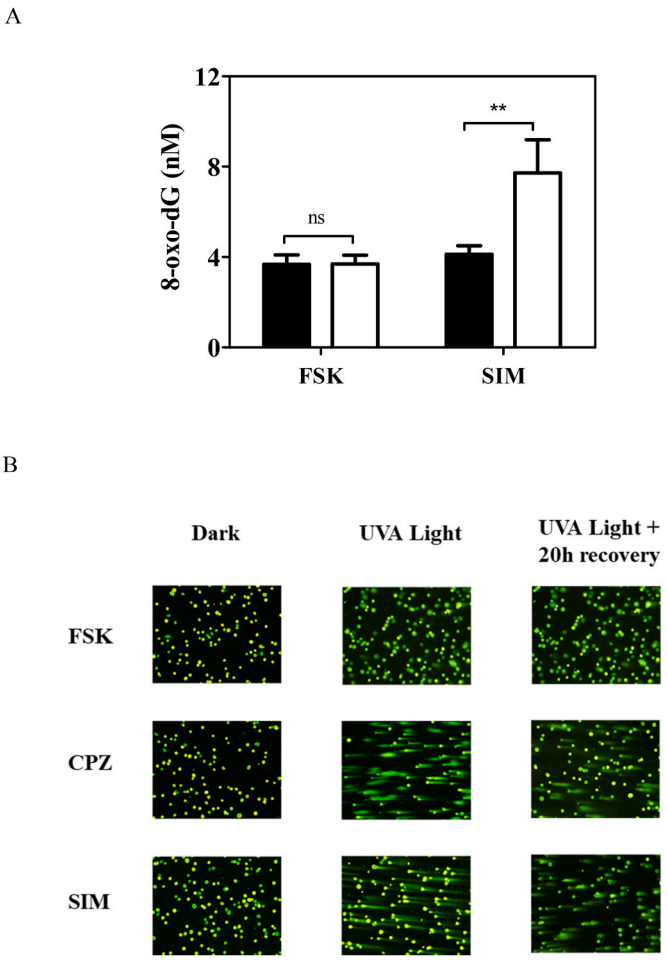

Fig. 4. Cellular photogenotoxicity. (A) 8-oxo-dG formation in human skin fibroblasts cells (FSK) upon SIM treatment. FSK cells alone (FSK) or treated with SIM (2.5 μM) were kept in Dark (■) or irradiated with a 2.5 J/cm^2 UVA dose (□). Then, genomic DNA was isolated and the oxidative biomarker 8-oxo-dG was quantified by means of colorimetric antibody Elisa assay. Asterisks indicate significant differences relative to the FSK cells in dark conditions by the Student's *t*-test (**$p < 0.01$; ns: non-significant). (B) Fluorescence microscopy images of SIM alkaline comet assay experiments. FSK cells alone (FSK) or treated with SIM (2.5 μM) or CPZ (10 μM) as the reference photogenotoxic compound were kept on dark conditions (Dark), irradiated with 2.5 J/cm^2 UVA dose (UVA Light) or irradiated with 2.5 J/cm^2 UVA dose followed by 20 h of cell recover (UVA Light + 20 h recovery time). Images are representative of three independent experiments.

of SIM to promote photooxidation in cellular membranes. According to our previous work on photosensitizing drugs [20,37], this type of HSA modification could involve a type I (radicals) or type II (singlet oxygen) photooxidation of the redox-active amino acid residues.

3.1.3. Photogenotoxicity

In order to evaluate whether DNA, another biomolecule target of oxidative damage, could also be involved in the SIM phototoxicity mechanism, a screening was performed using plasmid DNA alone or in combination with different repair enzymes (Endo V, Endo III and FPG). Actually, the electrophoresis agarose gel shown in Fig. S2 highlighted that SIM can indeed promote DNA photodamage mainly through purine base oxidation, as revealed using the FPG repair enzyme. Among all the oxidatively generated lesions into the cellular DNA by UVA light, one of the most frequent is the guanine residue oxidation at C8 to generate 8-oxo-7,8-dihydro-2′-deoxyguanosine (8-oxo-dG) [38]. This lesion can result highly mutagenic if it is not efficiently repaired, since this

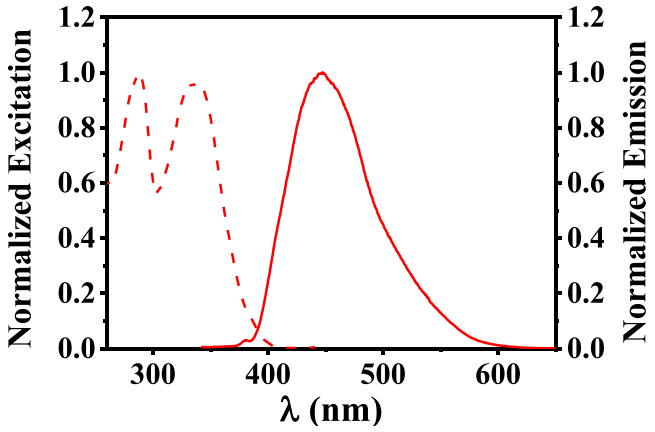

Fig. 5. Normalized fluorescence emission spectrum recorded at λ_{exc} = 332 nm (solid red) and normalized fluorescence excitation spectrum registered at λ_{max} = 447 nm (dashed red) of SIM in PBS solution. (For interpretation of the references to color in this figure legend, the reader is referred to the Web version of this article.)

modified base can pair in the double helix not only with cytosine but also with adenine. Having established the ability of SIM to induce purine oxidation in a cell-free system, in a further step, this process was also assessed in a cellular environment. Hence, the photogeneration of this biomarker in FSK cells DNA by SIM was studied. To achieve this goal, FSK were incubated with SIM and then, exposed to a UVA dose of 2.5 J/cm^2. After irradiation, genomic DNA was isolated and quantified by UV spectroscopy (λ=260 nm). Then, a competitive Elisa assay was carried out to detect the presence of 8-oxo-dG in samples. Thus, as shown in Fig. 4A, the 8-oxo-dG in SIM-treated cells was found to be twice higher than in non-treated cells. This agrees with the important role of guanine base oxidation in the photogenotoxicity of SIM.

In an attempt to describe in detail other types of DNA photolesions induced by SIM, comet assay experiments were subsequently carried out. This assay identifies combined DNA damage consisting of single-strand breaks, double-strand breaks, and alkali-labile sites on individual cells [39]. In this assay, after treatment with the drug and UVA irradiation, FSK cells were embedded in agarose mini-gels on slides and subjected to lysis. Afterwards, electrophoresis was run to allow damaged DNA fragments migrating out of the cell nucleus, forming a comet tail. Upon SYBR® Gold staining, comets and tail were examined under the fluorescence microscope and nuclear DNA damage was calculated using a visual score system of 6 different categories [27]. Moreover, chlorpromazine (CPZ), a well-known drug with photogenotoxic properties was used as positive control [18]. The results shown in Fig. 4B and Fig. S3 indicated that SIM generated significant DNA damage to cellular DNA (around 40%), to a lesser extent than CPZ. Additionally, another set of experiments were performed to investigate the capability of FSK cells to repair that DNA photodamage generated. For this purpose, cells upon treatment were incubated for different time periods up to 20 h and the remaining DNA damage was determined in the same way described above. As shown in Fig. 4B, in contrast to CPZ, it is noteworthy that photosensitized DNA was not repaired within 20 h of recovery. This is in agreement with the possibility of SIM to generate mutations in the DNA and ultimately, these could lead to photocarcinogenesis.

3.2. Photophysical studies

Drug photosensitizing potential can be associated with damage to biomolecules involving ROS or radicals arising from excited states [40]. Here, in order to gain insight into the phototoxicity of SIM, in a further step, photophysical studies combining fluorescence, transient absorption and time-resolved near-infrared luminescence spectroscopy were carried out.

3.2.1. Emission spectra

The steady-state fluorescence spectrum of SIM in PBS solution showed a maximum centered at λ_{max} = 447 nm (Fig. 5). The SIM fluorescence quantum yield (Φ_F) was determined using anthracene in ethanol as standard (Φ_F = 0.27) and it resulted to be *ca.* 0.05 [41] (Fig. S4). Similar results were obtained using MeCN and MeOH, as model solvent, mimicking lipophilic environment present in the cellular milieu (Table S1). In addition, singlet excited state energy (E_s) was calculated from the intersection between the normalized excitation and emission spectra (Fig. 5) and it was found to be 73.3 kcal/mol.

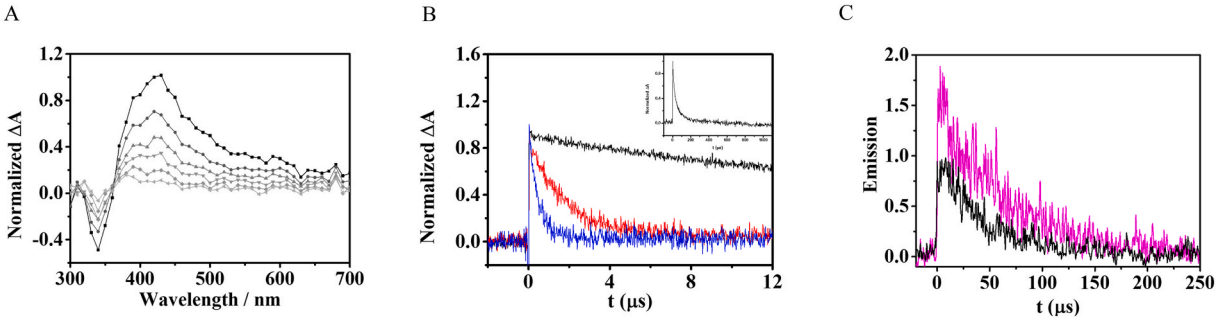

Fig. 6. Laser Flash Photolysis experiments. (A) Normalized transient absorption spectra (from 1 to 14 μs) for simeprevir in aerated PBS solution after the 355 nm laser excitation. (B) Normalized decay traces of the triplet generated in PBS solution of SIM monitored at 410 nm in deaerated (**black**), aerated (**red**) and oxygen saturated atmosphere (**blue**). Inset: normalized decay trace of SIM in deaerated PBS solution on a longer time-scale. (C) Kinetic traces for $^1O_2$ signals after laser pulse (λ_{exc} = 355 nm) for SIM in deuterated water (black). Tetramethyl-*p*-benzoquinone (DQ) in MeCN (**magenta**) was the reference of the study (Φ_Δ *ca.* 0.89). (For interpretation of the references to color in this figure legend, the reader is referred to the Web version of this article.)

3.2.2. Laser flash photolysis

To detect reactive species generated by the excitation of SIM living in the microsecond time-scale, laser flash photolysis (LFP) technique was employed. Thus, upon excitation of the drug at 355 nm in aerated PBS solution, the transient absorption spectrum exhibited a band with a maximum centered at 410 nm (Fig. 6A). In addition, from decay traces analysis at 410 nm it was determined the lifetime (τ_T) that was *ca.* 44 μs (Fig. 6B), and the triplet energy (E_T) obtained from phosphorescence measurements was approximately 59.6 kcal//mol (Fig. S5). Moreover, to characterize this transient species, oxygen quenching experiments were carried out in PBS solutions of the drug. As shown in Fig. 6B, this

species was efficiently quenched by molecular oxygen with a quenching rate constant (k_q) of 1.71 × 10^9 M^{-1} s^{-1} calculated by a mono-exponential decay function (Fig. S6). This indicates that the transient species peaking at 400 nm corresponds to a triplet excited state. For MeOH and MeCN solvents, comparable results were obtained (Fig. S7 and Table S1). Significant triplet production is indicative of potential photobiological damage since this excited state has a biradical character and is the precursor of the reactive species, including free radicals and ROS.

It is well known that a drug triplet excited state is usually regarded as the key precursor that sensitizes molecular singlet oxygen ($^1O_2$ or $^1\Delta g$) formation through an electronic energy transfer process in Type II oxidative mechanism reactions [42]. Furthermore, $^1O_2$ can promote extensive oxidative damage to biomolecules inside cells, including lipid peroxidation through hydroperoxide formation [24,25], protein oxidation [43], and DNA nucleosides (such as guanine) oxidation to obtain the final oxidized base (8-oxo-dG) [44]. Bearing in mind from cellular experiments that SIM promoted lipid photoperoxidation, protein photooxidation and 8-oxo-dG formation in DNA, the photogeneration of $^1O_2$ by this drug should be expected. To confirm this hypothesis, it is interesting to perform time-resolved near-infrared emission studies upon 355 nm excitation of SIM. Thus, formation of this species was detected by time-resolved measurements of the luminescence at 1270 nm in deuterated aqueous solution (Fig. 6C). To determine the SIM singlet oxygen quantum yield (Φ_Δ), tetramethyl-*p*-benzoquinone (DQ), was employed as reference (Φ_Δ *ca.* 0.89 in MeCN) [22]. As expected, SIM displayed ability to generate $^1O_2$ with a $\Phi_\Delta = 0.56$. The SIM Φ_Δ in organic solvents was also measured and they were found to be *ca.* 0.82 and 1 for MeOH and MeCN, respectively (Fig. S8 and Table S1). As regards the singlet oxygen lifetime (τ_Δ) in deuterated aqueous solution, it was measured using DQ as standard and was 65 μs. Likewise, the lifetime obtained for SIM was *ca.* 40 μs (Fig. 6C).

3.3. Molecular basis of simeprevir interaction with biomolecules

The photophysical studies of SIM are in good agreement with the cellular photodamage pointed out for this drug. This could be the origin of the oxidative stress to biomolecules, thus leading to undesired effects of phototoxicity and photogenotoxicity. Therefore, in view of the capability of SIM to form triplet excited species, it was considered convenient to perform additional experiments regarding SIM interaction with biomolecules, such as lipids, proteins and DNA. Thus, drug-lipid interaction studies were carried out by quenching experiments using 2-methylcyclohexa-2,5-dienecarboxylic acid (MBA) as a lipid model, which contains double allylic hydrogens and is an appropriate probe for studying the reactivity of lipids with photosensitizing drugs [43]. As a result, triplet decay traces were obtained in deaerated acetonitrile solutions of SIM after the addition of increasing amounts of MBA. As shown in Fig. 7, the SIM triplet species was quenched by MBA with a k_q of only 1.68 × 10^6 M^{-1} s^{-1} (Fig. 7, inset). Moreover, SIM-HSA (1:1) interaction did indeed occur, and the complex displayed a higher triplet lifetime ($\tau_T = 17$ μs) than the free drug in solution ($\tau_T = 1.7$ μs) under aerated atmosphere (Fig. S9 and Table S2). By contrast, τ_T of SIM in the presence of calf thymus DNA (ctDNA) remained unchanged; hence the complexation of SIM with DNA was not supported experimentally (Fig. S9 and Table S2).

Overall, the above data indicate that triplet quenching by oxygen, leading to singlet oxygen, is the predominating process in the presence of lipids and DNA; hence, photosensitized oxidation of these biomolecules occurs by a Type II mechanism. Conversely, in the presence of protein a complex is formed where the triplet state is protected from quenching by oxygen, and the formation of singlet oxygen is much less efficient (Table S2). Accordingly, under these conditions, oxidation of the proteins must proceed via a Type I mechanism. In view of the importance of SIM complexation to proteins, a detailed docking and molecular dynamics simulation study was performed on the binding process.

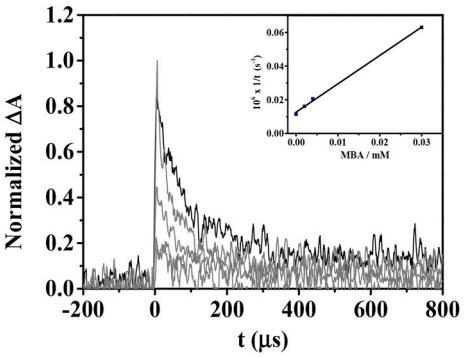

Fig. 7. Triplet decays at 410 nm for SIM alone (**black**) or in the presence of increasing amount of MBA (0–3 mM) (**gray**). Inset: Stern-Volmer plot for ^{3}SIM* quenching by MBA.

3.3.1. Binding of simeprevir to human serum albumin

To understand the underlying molecular basis of the interaction of SIM with the HSA protein, as well as its photophysical properties experimentally observed upon binding, docking and molecular dynamics (MD) simulation studies were performed.

In this context, HSA is a carrier protein with a large capacity for transporting a wide variety of endo and exogenous ligands structurally very diverse. It has three main recognition binding sites, namely domains I–III, each one divided into two sub-domains A and B, with a very different recognition pattern. Hence our first efforts were directed at identifying the SIM recognition domain of HSA, which was achieved by competition studies using three compounds whose protein binding sites are known, specifically ibuprofen (IBP) (site 1, sub-domain IIA), warfarin (WAF) (site 2, sub-domain IIIA) and lapatinib (LAP) (site 3, sub-domain IB) [45,33]. Thus, increasing amounts of the ligand were added to aerated solutions of 10 μM SIM-HSA (1:1), and transient decays were monitored at 410 nm. Under these conditions, a decrease of the transient species lifetime was only observed in parallel with the addition of LAP concomitantly with an increase of the free SIM fraction (k_q of *ca.* 5.1 × 10^9 $M^{-1}s^{-1}$), ergo, this can be correlated with the complexation of SIM to the binding site 3 of HSA (Fig. 8A and Fig. S10). Thus, to determine the binding constant of SIM to HSA, the decays monitored at 410 nm were fitted using a two-phase exponential function. Then, using the preexponential factors values, both the percentage of free and bound SIM were calculated (Fig. S10). The half-maximal effective concentration (EC50) for lapatinib was obtained by interpolation from competition displacement curve and it resulted to be 7 μM (Fig. 8B). Moreover, the binding constant of lapatinib to HSA (K_B) was taken from the literature and it was 1.24 × 10^5 M^{-1} (at 303 K) [46]. As the SIM concentration used was 10 μM, the relationship between the binding constants was found to be 0.7 and therefore the K_B of SIM resulted to be 0.87 10^5 M^{-1}.

Based on the results obtained with the afore-mentioned competition studies, through which site 3 (sub-domain IB) was identified as the SIM binding pocket, the three-dimensional structure of HSA in complex with myristic acid and hemin (PDB ID 1O9X) was selected for docking. Among the variety of HSA crystal structures available, this PDB was chosen because hemin, as well as LAP, binds to sub-domain IB. It is important to note that this protein undergoes significant conformational changes, especially in domains I and III, both located at the vertices of its general V-shaped structure, to maximize its interaction with ligands [47]. Hence, choosing a PDB with a ligand already arranged in the same pocket becomes relevant for achieving optimal docking results. In addition, performing MD simulation studies on the proposed ligand@HSA binary complex, through which the intrinsic plasticity of the protein is considered, is also relevant for achieving reliable and

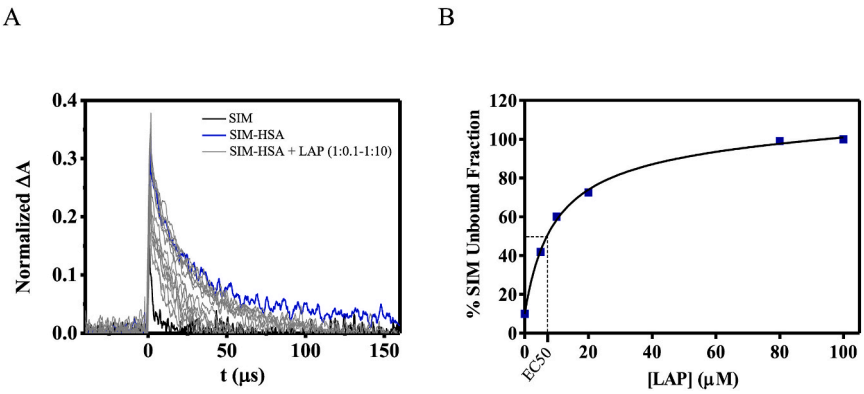

Fig. 8. A) Decays at 410 nm for SIM (**black**), SIM-HSA alone (**blue**) or in the presence of increasing amounts of LAP (**gray**). B) Percentage of unbound SIM fraction at 1:1 SIM-HSA ratio in the presence of increasing amounts of LAP. (For interpretation of the references to color in this figure legend, the reader is referred to the Web version of this article.)

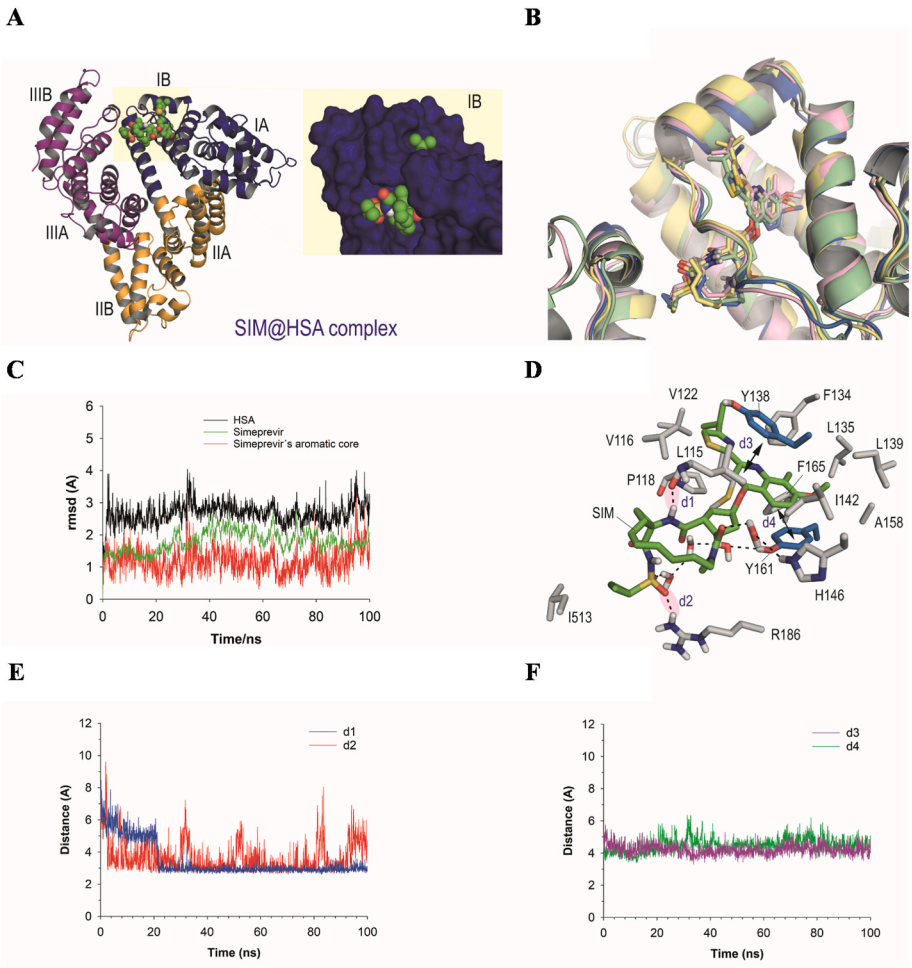

Fig. 9. SIM binding mode against HSA protein obtained by MD simulation studies. (A) General and close views of the SIM@HSA binary complex. Snapshot taken after 80 ns of simulation. The domains (I–III) and sub-domains (A, B) of the protein are shown in blue, orange, and purple colors, respectively, and labeled. Note how SIM (spheres) is deeply buried in sub-domain IB (site 3) of the protein. (B) Superposition of several snapshots taken during the whole simulation. Note how the ligand is very stable within the pocket as no relevant changes are identified. (C) RMSD plots for the protein backbone (Cα, C, O and N atoms), SIM and its quinoline core (average values of 1.8 Å, 2.7 Å and 1.2 Å, respectively). (D) Main contacts of SIM with the protein. Relevant hydrogen bonding interactions (black dashed lines) and protein residues are shown and labeled. (E) Stability of the hydrogen bonding interactions. Variation of the relative distances between the NH amide group of the ligand and the main carbonyl group of L115 (d1) and the oxygen atom of the sulfonamide group of the ligand and the guanidinium group of R186 (d2). (F) Stability of the π-π stacking interactions. Variation of the relative distances between the center of mass of quinoline ring of SIM and residues Y138 (d3, average distance of 4.2 Å) and Y161 (d4, average distance of 4.6 Å) during the whole simulation. For calculating average distances, only the last 80 ns of simulation are considered. (For interpretation of the references to color in this figure legend, the reader is referred to the Web version of this article.)

realistic results. To this end, the highest score solution obtained by docking and the protein were immersed in a truncated octahedron of water molecules obtained with the molecular mechanics force field Amber and subjected to 100 ns of simulation.

Our simulation studies revealed that SIM would be buried in sub-domain IB of the protein through its quinoline group allocating its macrocyclic moiety pointing towards the interface between domains I and III (Fig. 9A). The ligand proved to be very stable in the pocket, since no significant changes were observed, either in the binding conformation of the ligand or that of the SIM@HSA binary complex, during the whole simulation (Fig. 9B). Thus, the analysis of the root-mean-square deviation (rmsd) of the protein backbone (Cα, C, O and N atoms), the ligand and its quinoline group afforded low average values of 1.8 Å, 2.7 Å and 1.2 Å, respectively, for the whole simulation (Fig. 9C). SIM would be anchored to sub-domain IB through two hydrogen bonding interactions, one between the amide NH group in the SIM's macrocycle moiety and the main carbonyl group of L115, and the second between its sulfonamide group and the guanidinium group of

R186 (Fig. 9D). The latter interactions proved to be very stable, showing average distances during the last 80 ns of simulation of 3.0 Å and 3.5 Å, respectively (Fig. 9E). Additional hydrogen bonds are also established by the ligand through both faces of its macrocycle moiety with the side chains of residues H146 and Y161 via a network of water molecules. The arrangement of the ligand is further stabilized within the pocket by a strong sandwich-like π-π stacking interaction with residues Y138 and Y161 that trap the quinoline moiety between them. The latter interaction revealed to be strong as no significant variation of the relative distances between the center of mass of the quinoline ring and the phenol groups in Y138 and Y161 was observed during the whole simulation (Fig. 9F). Finally, the ligand is further stabilized in subdomain IB thanks to a set of hydrophobic interactions with the nonpolar residues of the pocket, specifically L115, V116, P118, V122, F134, L135, L139, I142, A158 and I513.

4. Conclusions

Comprehensive photochemical and photobiological studies reveal SIM-mediated photodamage to biomolecules, leading ultimately to cell death. This drug displays a significant absorption band in the active region of solar light, so it may trigger photosensitivity reactions. The key transient species generated upon SIM irradiation is the triplet excited state, characterized by its absorption band at 400 nm. This species is efficiently quenched by oxygen giving rise to singlet oxygen, which is responsible for the oxidation of lipids and DNA (Type II mechanism). In the presence of HSA, the photobehavior is dominated by binding to site 3 of the protein, to give a stable SIM@HSA complex. Inside the complex, quenching of the triplet excited state is less efficient, which results in a longer triplet lifetime and in a deceased singlet oxygen formation. Hence, SIM-mediated photooxidation of the protein occurs through a radical (Type I) mechanism.

In summary, the obtained results confirm that porphyrin elevation in patients treated with SIM may not be the only mechanism responsible for SIM-associated clinical photosensitivity. Instead, photochemical mechanisms may operate leading to the generation of cellular oxidative stress associated with damage to lipids, proteins and DNA, ultimately resulting in cellular photo(geno)toxicity. These considerations have to be taken into account by the doctors to have a better knowledge of the SIM photoinduced adverse effects before prescribing to patients and, thus, give them photoprotection guidelines such as the employment of sunscreens.

Acknowledgments

Financial support from the Spanish Ministry of Science and Innovation [PID2020-115010RB-I00/AEI/10.13039/501100011033 (I.A), PID2019-105512RB-I00/AEI/10.13039/501100011033 (CG-B) and FPU predoctoral fellowship for M. El O.], Axencia Galega de Innovación (2020-PG067, CG-B), the Xunta de Galicia [ED431C 2021/29 and the Centro singular de investigación de Galicia accreditation 2019–2022 (ED431G 2019/03),], and the European Regional Development Fund (ERDF) is gratefully acknowledged. All authors are grateful to the Centro de Supercomputación de Galicia (CESGA) for use of the Finis Terrae computer.

Appendix A. Supplementary data

Supplementary data to this article can be found online at https://doi.org/10.1016/j.freeradbiomed.2022.11.006.

References

[1] F. Negro, A. Alberti, The global health burden of hepatitis C virus infection, Liver Int. 31 (Suppl 2) (2011) 1–3.
[2] W.H.O. Hepatitis, C Fact Sheet No 164, 2013 [cited 2021 2 December].
[3] A. Petruzziello, et al., Global epidemiology of hepatitis C virus infection: an up-date of the distribution and circulation of hepatitis C virus genotypes, World J. Gastroenterol. 22 (34) (2016) 7824–7840.
[4] T.I. Lin, et al., In vitro activity and preclinical profile of TMC435350, a potent hepatitis C virus protease inhibitor, Antimicrob. Agents Chemother. 53 (4) (2009) 1377–1385.
[5] M. Sanford, Simeprevir: a review of its use in patients with chronic hepatitis C virus infection, Drugs 75 (2) (2015) 183–196.
[6] R. Flisiak, J. Pogorzelska, M. Flisiak-Jackiewicz, Hepatitis C: efficacy and safety in real life, Liver Int. 37 (Suppl 1) (2017) 26–32.
[7] Z. Mariño, et al., High efficacy of Sofosbuvir plus Simeprevir in a large cohort of Spanish cirrhotic patients infected with genotypes 1 and 4, Liver Int. 37 (12) (2017) 1823–1832.
[8] M.V. Lin, R. Chung, Recent FDA approval of sofosbuvir and simeprevir. Implications for current HCV treatment, Clin Liver Dis (Hoboken) 3 (3) (2014) 65–68.
[9] H.S. Lo, et al., Simeprevir potently suppresses SARS-CoV-2 replication and synergizes with remdesivir, ACS Cent. Sci. 7 (5) (2021) 792–802.
[10] F.S. Hosseini, M. Amanlou, Anti-HCV and anti-malaria agent, potential candidates to repurpose for coronavirus infection: virtual screening, molecular docking, and molecular dynamics simulation study, Life Sci. 258 (2020), 118205.
[11] M.A. Bakowski, et al., Drug repurposing screens identify chemical entities for the development of COVID-19 interventions, Nat. Commun. 12 (1) (2021) 3309.
[12] Z.W. Eyre, A.M. Secrest, J.L. Woodcock, Photo-induced drug eruption in a patient on combination simeprevir/sofosbuvir for hepatitis C, JAAD Case Rep 2 (3) (2016) 224–226.
[13] C.L. Simpson, D. McCausland, E.Y. Chu, Photo-distributed lichenoid eruption secondary to direct anti-viral therapy for hepatitis C, J. Cutan. Pathol. 42 (10) (2015) 769–773.
[14] F. Borgia, et al., Mucocutaneous toxicity during simeprevir treatment for hepatitis C. A single institution, retrospective case series, Br. J. Clin. Pharmacol. 83 (5) (2017) 1152–1154.
[15] M.P. Manns, et al., Simeprevir with peginterferon/ribavirin for treatment of chronic hepatitis C virus genotype 1 infection: pooled safety analysis from Phase IIb and III studies, J. Viral Hepat. 22 (4) (2015) 366–375.
[16] L. Boglione, et al., Role of simeprevir plasma concentrations in HCV treated patients with dermatological manifestations, Dig. Liver Dis. 49 (6) (2017) 705–708.
[17] L.D. Crow, et al., Medications associated with increased risk of keratinocyte carcinoma, Dermatol. Clin. 37 (3) (2019) 297–305.
[18] F. Palumbo, et al., Enhanced photo(geno)toxicity of demethylated chlorpromazine metabolites, Toxicol. Appl. Pharmacol. 313 (2016) 131–137.
[19] G. Garcia-Lainez, et al., Photo(geno)toxicity changes associated with hydroxylation of the aromatic chromophores during diclofenac metabolism, Toxicol. Appl. Pharmacol. 341 (2018) 51–55.
[20] G. García-Lainez, et al., In vitro assessment of the photo(geno)toxicity associated with Lapatinib, a Tyrosine Kinase inhibitor, Arch. Toxicol. 95 (1) (2021) 169–178.
[21] L. Tamarit, et al., Photoprocesses of the tyrosine kinase inhibitor gefitinib: from femtoseconds to microseconds and from solution to cells, Chem. Sci. 12 (36) (2021) 12027–12035.
[22] I. Gutiérrez, S.G. Bertolotti, M.A. Biasutti, A.T. Soltermann, N.A. García, Quinones and hydroxyquinones as generators and quenchers of singlet molecular oxygen, Can. J. Chem. 75 (4) (1997) 423–428.
[23] OECD, Test No. 432, in: Vitro 3T3 NRU Phototoxicity Test, 2019.
[24] E.H. Pap, et al., Ratio-fluorescence microscopy of lipid oxidation in living cells using C11-BODIPY(581/591), FEBS Lett. 453 (3) (1999) 278–282.
[25] I.O.L. Bacellar, M.S. Baptista, Mechanisms of photosensitized lipid oxidation and membrane permeabilization, ACS Omega 4 (26) (2019) 21636–21646.
[26] G. Colombo, et al., A step-by-step protocol for assaying protein carbonylation in biological samples, J. Chromatogr., B: Anal. Technol. Biomed. Life Sci. 1019 (2016) 178–190.
[27] P. Møller, Assessment of reference values for DNA damage detected by the comet assay in human blood cell DNA, Mutat. Res. 612 (2) (2006) 84–104.
[28] I. Vaya, et al., Characterization of locally excited and charge-transfer states of the anticancer drug lapatinib by ultrafast spectroscopy and computational studies, Chemistry 26 (68) (2020) 15922–15930.
[29] I. Andreu, et al., Protein binding of lapatinib and its N- and O-dealkylated metabolites interrogated by fluorescence, ultrafast spectroscopy and molecular dynamics simulations, Front. Pharmacol. 11 (2020), 576495.
[30] P.A. Zunszain, et al., Crystal structural analysis of human serum albumin complexed with hemin and fatty acid, BMC Struct. Biol. 3 (1) (2003) 6.
[31] G. Jones, et al., Development and validation of a genetic algorithm for flexible docking11Edited by F. E. Cohen, J. Mol. Biol. 267 (3) (1997) 727–748.
[32] O. Molins-Molina, et al., Photobinding of triflusal to human serum albumin investigated by fluorescence, proteomic analysis, and computational studies, Front. Pharmacol. 10 (2019) 1028.
[33] D. Case, et al., Amber 2017, University of California, San Francisco, 2017.
[34] J. Cadet, K.J.A. Davies, Oxidative DNA damage & repair: an introduction, Free Radic. Biol. Med. 107 (2017) 2–12.
[35] G.P. Drummen, et al., C11-BODIPY(581/591), an oxidation-sensitive fluorescent lipid peroxidation probe: (micro)spectroscopic characterization and validation of methodology, Free Radic. Biol. Med. 33 (4) (2002) 473–490.
[36] M. Laguerre, J. Lecomte, P. Villeneuve, Evaluation of the ability of antioxidants to counteract lipid oxidation: existing methods, new trends and challenges, Prog. Lipid Res. 46 (5) (2007) 244–282.

[37] L. Tamarit, et al., Photoprocesses of the tyrosine kinase inhibitor gefitinib: from femtoseconds to microseconds and from solution to cells, Chem. Sci. 12 (36) (2021) 12027–12035.
[38] J. Bai, et al., Oxidation of 8-Oxo-7,8-dihydro-2'-deoxyguanosine leads to substantial DNA-histone cross-links within nucleosome core particles, Chem. Res. Toxicol. 31 (12) (2018) 1364–1372.
[39] A. Azqueta, A.R. Collins, The essential comet assay: a comprehensive guide to measuring DNA damage and repair, Arch. Toxicol. 87 (6) (2013) 949–968.
[40] K. Nakai, D. Tsuruta, What are reactive oxygen species, free radicals, and oxidative stress in skin diseases? Int. J. Mol. Sci. 22 (19) (2021).
[41] W.H. Melhuish, Quantum efficiencies of fluorescence of organic substances: effect of solvent and concentration of the fluorescent solute1, J. Phys. Chem. 65 (2) (1961) 229–235.
[42] S. Hackbarth, et al., New insights to primary photodynamic effects–Singlet oxygen kinetics in living cells, J. Photochem. Photobiol., B 98 (3) (2010) 173–179.
[43] M.J. Davies, Singlet oxygen-mediated damage to proteins and its consequences, Biochem. Biophys. Res. Commun. 305 (3) (2003) 761–770.
[44] M.S. Baptista, et al., Type I and type II photosensitized oxidation reactions: guidelines and mechanistic pathways, Photochem. Photobiol. 93 (4) (2017) 912–919.
[45] W.L. DeLano, The PyMOL Molecular Graphics System, 2002.
[46] M.Z. Kabir, et al., Characterization of the binding of an anticancer drug, lapatinib to human serum albumin, J. Photochem. Photobiol., B 160 (2016) 229–239.
[47] S. Curry, et al., Crystal structure of human serum albumin complexed with fatty acid reveals an asymmetric distribution of binding sites, Nat. Struct. Biol. 5 (9) (1998) 827–835.